# Unraveling the Potential of Matrix Transformers in High-Current Low-Voltage Applications

Dr. Jannik Schäfer
*Power Electronic Systems Laboratory*
*ETH Zurich*
Zurich, Switzerland
schaefer@lem.ee.ethz.ch

Prof. Dr. Johann W. Kolar
*Power Electronic Systems Laboratory*
*ETH Zurich*
Zurich, Switzerland
kolar@lem.ee.ethz.ch

**This paper aims to advance the understanding and application of matrix transformers in contemporary power electronics based on the exemplary specifications of an electric vehicle high-current/low-voltage DC/DC step-down converter. First, the general applicability of matrix transformer arrangements in power electronic systems is investigated, providing a nuanced discussion on scenarios where they outperform conventional transformer designs. Subsequently, the two principal types of matrix transformers: common-voltage and common-current matrix transformers are introduced, emphasizing the distinctive features that set them apart. A comprehensive analysis of the electromagnetic behavior of the two matrix transformer types is presented, highlighting their unique characteristics and advantages. Concluding the discussion, practical design suggestions are presented to maximize the potential of matrix transformers, enhancing the efficiency and power density of power electronic systems.**

## I. Introduction

In power electronic applications where electrical energy must be transferred either between galvanically isolated energy sources and loads and/or between energy sources and loads with significantly different voltage levels, a transformer is often employed. If the power electronic converter links only two voltage levels, the transformer typically consists of two windings (a primary winding $P$ and a secondary winding $S$) that are magnetically coupled through a magnetically conductive core $C$ (cf. **Figs. 1ab**) [1,2]. In most cases, with this conventional configuration, it is possible to design highly efficient and compact transformers for a wide range of operating frequencies [3].

However, under certain conditions, employing more complex transformer arrangements, where individual windings are split and then connected in series or parallel, results in significantly more compact and efficient transformer designs, cf. **Fig. 1c** [4]–[6]. Such transformer structures are commonly referred to as matrix transformers (MTs) and can be broadly categorized into two types: common-voltage matrix transformers (CVMTs), as shown in **Fig. 1d**, and common-current matrix transformers (CCMTs) as shown in **Fig. 1e**. Before delving into the distinctions and similarities of the two MT categories in **Section III**, **Section II** discusses the situations or conditions under which the use of matrix transformers should generally be considered. Subsequently, the structure, the design and the advantages of CCMTs and the CVMTs are analyzed in detail in **Section IV** and **Section V**, respectively. Finally, **Section VI** concludes the paper.

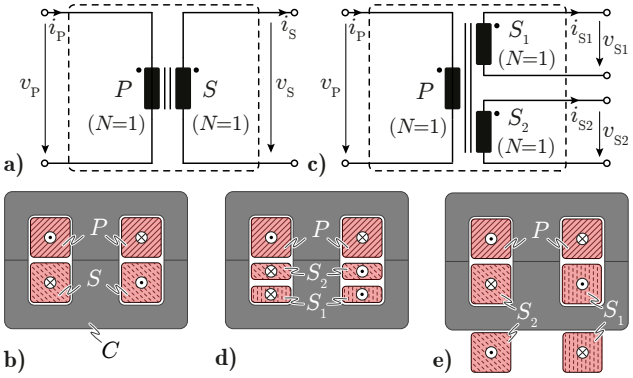


**Fig. 1.** Equivalent circuit diagram **(a)** and cross-section **(b)** of a conventional transformer with two windings $P$ and $S$, magnetically coupled through two E-cores $C$. In **(c)**, the equivalent circuit diagram of a matrix transformer with a split secondary winding is depicted. **(d)** illustrates the cross-section of an implementation of this matrix transformer as a Common-Voltage Matrix Transformer (CVMT), while **(e)** represents the implementation as a Common-Current Matrix Transformer (CCMT).

## II. Applications in which Matrix Transformers should be used

The size of a transformer, simplistically speaking, depends on two main quantities: the maximum (rms) current in the primary and secondary windings $I_X, X \in \{P,S\}$, and the maximum applied voltage-time areas $\psi_X$. The latter are defined by the maximum applied winding voltages $V_X$ and the switching frequency $f_{sw}$ and can be estimated according to $\psi_X = {}^{V_X}/_{2\cdot f_{sw}}$. In most converter systems, the transformer's secondary windings are connected to a rectifier circuit and are thus directly connected to a voltage source $V_S$, whereas the primary winding is connected to the often higher voltage and/or lower current primary side through a series inductor, e.g. required for resonant operation. Consequently, the magnetizing flux in the transformer is primarily determined by the secondary-side voltage $V_S$, which is why the subsequent analysis focuses on the secondary-side quantities $\psi_S$ and $I_S$. Taking into account a

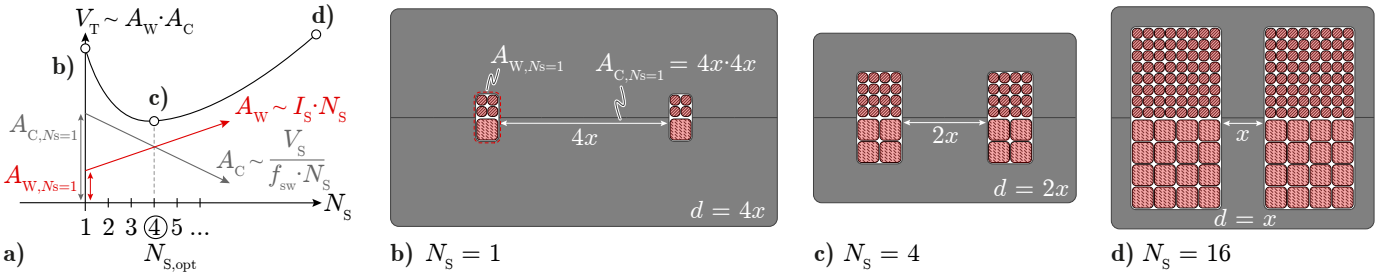


**Fig. 2.** **(a)** Qualitative scaling law of the volume of a conventional transformer, along with three transformer designs with an exemplary winding ratio (n) of 4:1 and different numbers of secondary turns $N_S$ in **(b)**, **(c)**, and **(d)**, in order to visually illustrate the scaling law of **(a)**.

maximum permissible current density $J_{max}$ imposed by thermal limitations in the windings, $I_S$ directly defines the minimum required effective winding window $A_{W,Ns=1}$ for a secondary winding with a single turn (cf. **Fig. 2b**), according to [1,2]

$$A_{W,Ns=1} = \frac{2 \cdot I_S}{k_W \cdot J_{max}}, \tag{1}$$

where $k_W$ denotes the winding filling factor, which is assumed to be 1 for all further calculations for simplicity reasons. Similarly, the minimum required core cross-sectional area $A_{C,Ns=1}$ for a secondary winding with a single turn can be calculated based on the maximum applied voltage-time area as well as the saturation flux-density $B_{sat}$ of the core material, according to [1,2]

$$A_{C,Ns=1} = \frac{V_S}{2 \cdot f_{sw} \cdot B_{sat}}. \tag{2}$$

In most applications, the ratio between $\psi_S$ and $I_S$ is such that for a secondary winding with only one turn ($N_S = 1$), a very small winding window $A_{W,Ns=1}$ is required. However, a core with an extremely large cross-sectional area must be employed to prevent saturation of the core material (cf. **Fig. 2b**). This results in a large total transformer volume $V_T$. To reduce the core size, a higher number of secondary turns $N_S$ can be used. Although this increases the required winding window $A_W$, it proportionally reduces the core cross-sectional area $A_C$, whereby the overall $V_T$ is decreasing (cf. **Fig. 2c**). However, if $N_S$ is increased too much, the winding volume starts to dominate, leading to an overall increase in $V_T$ again (cf. **Fig. 2d**). Therefore, there exists an optimal number of secondary turns $N_{S,opt}$ for which $V_T$ is minimized (cf. **Fig. 2a**).

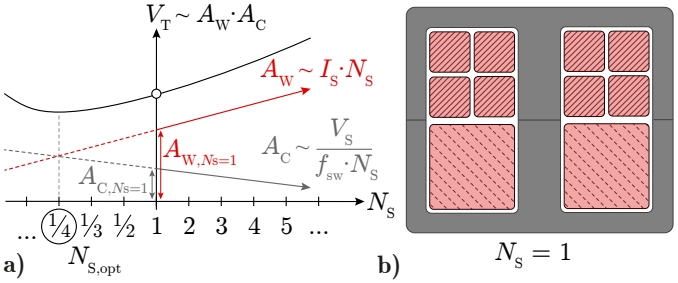


**Fig. 3.** **(a)** Qualitative scaling law of the volume of a conventional transformer in low output voltage/large output current applications, and **(b)** a transformer design with an exemplary winding ratio (n) of 4:1 in order to visually illustrate the respective scaling law.

However, there are applications whose specifications lead to the scenario where even for $N_S = 1$, the winding volume dominates (cf. **Fig. 3**). In such cases, one would ideally need to further decrease $N_S$ to minimize the transformer volume. This situation often arises in applications where very high currents ($I_S$) need to be delivered at very low output voltages ($V_S$). However, reducing $N_S$ further would imply using fractional turns, i.e., $N_S < 1$, which proves challenging with conventional transformer structures.

At this point, the aforementioned matrix transformers (MT) come into play, as some of these transformer structures allow to extend the design space into the region $N_S < 1$. This is achieved by splitting the secondary winding into several, ultimately parallel-connected, sub-windings, which are magnetically coupled to the primary winding in different ways (cf. **Fig. 1c**). The impact of these rearrangements on the electrical behavior of the transformer will be analyzed in detail in the next section.

## III. Electromagnetic Behavior of Different Types of Matrix Transformers

As mentioned earlier, there are two types of matrix transformers (MTs): common-voltage matrix transformers (CVMTs), as depicted in **Fig. 1d**, and common-current matrix transformers (CCMTs), as shown in **Fig. 1e**. To correctly classify a specific MT arrangement into the appropriate type, it is sufficient to examine the time derivative of the magnetic flux through the respective windings and the currents through the winding windows.

Neglecting any potential leakage flux in the transformer and assuming an infinite relative permeability of the core material, Ampère's law leads to the condition that the total current in a winding window must be zero, or equivalently, that all currents in a winding window must cancel each other out. Due to this condition, the ratios between the currents in the different windings can be directly derived. The analysis of the left winding window of the MT in **Fig. 1d**, for example, thus leads to the conclusion that the sum of the two currents in the

secondary windings $S_1$ and $S_2$ must be equal the current in the primary winding $P$, or generally

$$N_\mathrm{P} \cdot i_\mathrm{P} = N_{\mathrm{S},1} \cdot i_{\mathrm{S},1} + N_{\mathrm{S},2} \cdot i_{\mathrm{S},2}. \tag{3}$$

The analysis of the second winding window is redundant as it leads to the same conclusion. If the two winding windows of the MT in **Fig. 1e** are analyzed, the following two relationships can be found:

$$N_\mathrm{P} \cdot i_\mathrm{P} = N_{\mathrm{S},1} \cdot i_{\mathrm{S},1} \qquad \text{and} \qquad N_\mathrm{P} \cdot i_\mathrm{P} = N_{\mathrm{S},2} \cdot i_{\mathrm{S},2}. \tag{4}$$

In other words, due to the magnetic coupling of the windings, the two secondary currents are always identical (if $N_{\mathrm{S},1} = N_{\mathrm{S},2}$ is assumed), which is why this arrangement is referred to as a common-current MT (CCMT).

To find the ratios of the induced voltages in the windings, the time derivatives of the magnetic fluxes through the respective windings, or generally, the fluxes through the windings, are compared with each other. In the case of the MT in **Fig. 1d**, all windings are wound around the center leg of the E-core and consequently experience the same magnetic flux, which is why the voltage ratios are given according to

$$\frac{v_\mathrm{P}}{N_\mathrm{P}} = \frac{\mathrm{d}\varphi_\mathrm{P}}{\mathrm{d}t} = \frac{\mathrm{d}\varphi_{\mathrm{S},1}}{\mathrm{d}t} = \frac{v_{\mathrm{S},1}}{N_{\mathrm{S},1}} \tag{5}$$

and

$$\frac{v_\mathrm{P}}{N_\mathrm{P}} = \frac{\mathrm{d}\varphi_\mathrm{P}}{\mathrm{d}t} = \frac{\mathrm{d}\varphi_{\mathrm{S},2}}{\mathrm{d}t} = \frac{v_{\mathrm{S},2}}{N_{\mathrm{S},2}}. \tag{6}$$

Since, assuming $N_{\mathrm{S},1} = N_{\mathrm{S},2}$, the two secondary voltages are identical, MTs with this winding arrangement are referred to as common-voltage MTs (CVMTs).

In the MT of **Fig. 1e**, the flux $\varphi_\mathrm{P}$ induced by the primary winding is divided between the two outer limbs, with one part of the flux ($\varphi_{\mathrm{S}1}$) flowing through winding $S_1$ and the other part ($\varphi_{\mathrm{S}2}$) through winding $S_2$. Since the sum of the two partial fluxes $\varphi_{\mathrm{S}1}$ and $\varphi_{\mathrm{S}2}$ must be equal to $\varphi_\mathrm{P}$, the sum of the two secondary induced voltages must correspond to the primary voltage as well:

$$\frac{v_\mathrm{P}}{N_\mathrm{P}} = \frac{\mathrm{d}\varphi_\mathrm{P}}{\mathrm{d}t} = \frac{\mathrm{d}\varphi_{\mathrm{S},1}}{\mathrm{d}t} + \frac{\mathrm{d}\varphi_{\mathrm{S},2}}{\mathrm{d}t} = \frac{v_{\mathrm{S},1}}{N_{\mathrm{S},1}} + \frac{v_{\mathrm{S},2}}{N_{\mathrm{S},2}}. \tag{7}$$

Comparing the voltage transformation ratios of a CVMT and a CCMT with parallel-connected secondary windings ($v_{\mathrm{S},1} = v_{\mathrm{S},2} = v_\mathrm{S}$), whereby potential leakage fluxes are neglected and a symmetric transformer structure as well as $N_\mathrm{P} = N_{\mathrm{S},1} = N_{\mathrm{S},2} = 1$ is assumed, the following ratios are found:

$$\frac{v_\mathrm{S}}{v_\mathrm{P}}(\mathrm{CVMT}) = \frac{1}{1} \qquad \text{and} \qquad \frac{v_\mathrm{S}}{v_\mathrm{P}}(\mathrm{CCMT}) = \frac{1}{2}. \tag{8}$$

Hence, while a CVMT divides the secondary winding and distributes the total current across multiple individual windings, it does not affect the voltage transformation ratio. Therefore, the issue depicted in **Fig. 3a**, where a $N_\mathrm{S} < 1$ would be desired, cannot be resolved with this configuration. However, this can be achieved with CCMTs, since two parallel-connected windings, each with one turn, collectively behave like a single winding with half a turn. This concept can be scaled arbitrarily, for example, by using a core with three return paths (core limbs) for the primary side induced magnetic flux and three parallel-connected secondary windings, which collectively behave like a single winding with one-third of a turn. This will be explained in more detail in the following section.

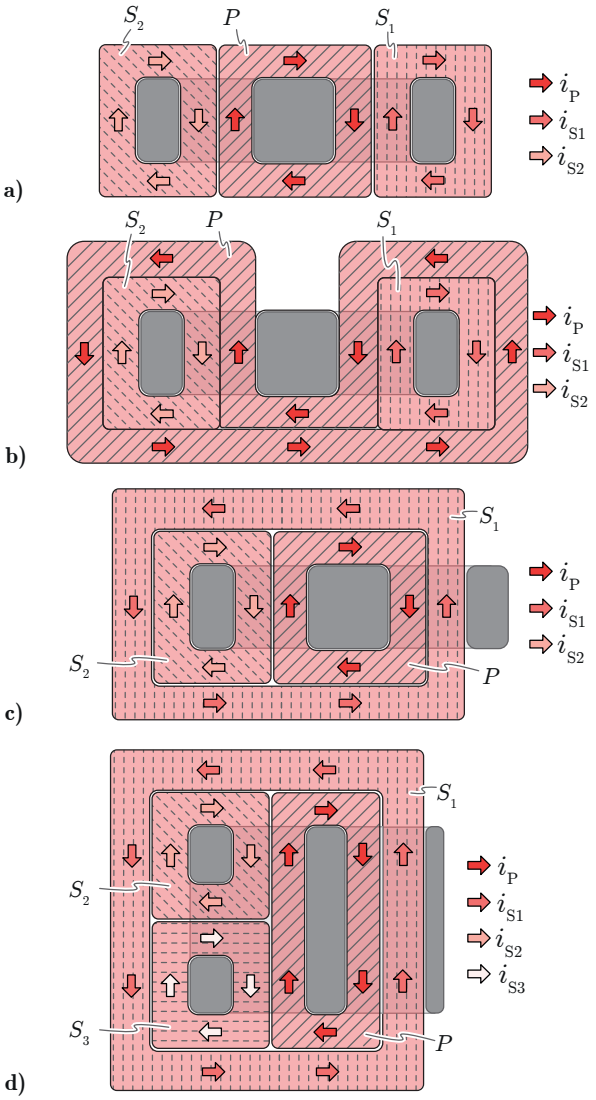


**Fig. 4. (a)** Top view of a CCMT with an E-core and two secondary windings with the respective current directions, **(b)** the same transformer but with the conventional HF optimized winding arrangement with a rearranged primary winding and **(c)** the same but HF and design implementation optimized CCMT with a rearranged secondary winding $S_1$. **(d)** Optimized CCMT with a third secondary winding $S_3$.

## IV. Optimal Design of Common-Current Matrix Transformers

As shown previously, CCMTs allow for the design of secondary windings with fractional turns. This is achieved by providing multiple parallel return paths for the primary side induced magnetic flux, with a secondary winding arranged

around each return path. Such an exemplary arrangement is depicted again in **Fig. 4a**, where two secondary windings $S_1$ and $S_2$ are arranged around the two return paths (outer limbs) of a conventional E-core, where the primary winding $P$ is wound around the center leg.

Even though this arrangement leads to the desired electromagnetic behavior of the transformer, where the effective secondary side number of turns $N_{\mathrm{S,eff}}$ corresponds to $1/2$, the efficiency of the transformer in practical applications would be limited. This is especially true since CCMTs are used in high current applications where large effective copper cross-sectional areas are required. These are known to be susceptible to high-frequency (HF) conduction losses caused by eddy currents induced by internally generated (skin effect) or externally applied (proximity effect) magnetic fields. As is well known, these magnetic fields and thus the HF conduction losses in conventional transformers can be minimized by winding the primary ($P$) and secondary ($S$) windings on top of each other. This results in the antiparallel flow of currents $i_{\mathrm{P}}$ and $i_{\mathrm{S}}$ along the entire length of the winding, causing the magnetic field to practically vanish in at least one dimension, greatly simplifying the HF design of such magnetic components (cf. **Fig. 5**). Unfortunately, in the CCMT of **Fig. 4a**, this antiparallel current flow occurs only in the winding windows, while outside the core, only one of the currents $i_{\mathrm{P}}$, $i_{\mathrm{S1}}$ or $i_{\mathrm{S2}}$ flows at a time. This inevitably leads to significant HF conduction losses, which, however, can be relatively easily minimized by rearranging either the primary winding as shown in **Fig. 4b**, or alternatively, the secondary winding $S_1$ as shown in **Fig. 4c**. The second option not only enhances the HF performance of the arrangement but also simplifies the practical implementation as a PCB-winding transformer, especially if blind and buried vias should be avoided. However, this paper does not delve into this aspect in detail, as its primary focus is on the conceptual aspects.

From a magnetic perspective, the behavior of the transformer does not change with the relocation of $S_1$. However, the efficiency in terms of HF losses is significantly improved, as now on each subsection of the windings, two antiparallel currents can be found, partially compensating for their magnetic fields. Thus, the advantageous HF conditions of a conventional transformer are also achieved in a CCMT.

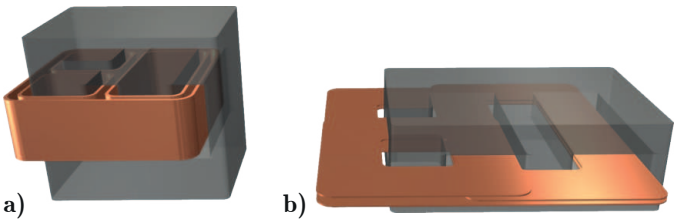


**Fig. 5.** **(a)** Exemplary practical implementation of the CCMT of **Fig. 4c** with single-turn foil windings and **(b)** the same MT but with PCB-integrated single-turn windings, where the windings are not placed next to each other as shown in **Fig. 4c**, but on top of each other for efficiency reasons. The windings are shown without their terminals for the sake of clarity.

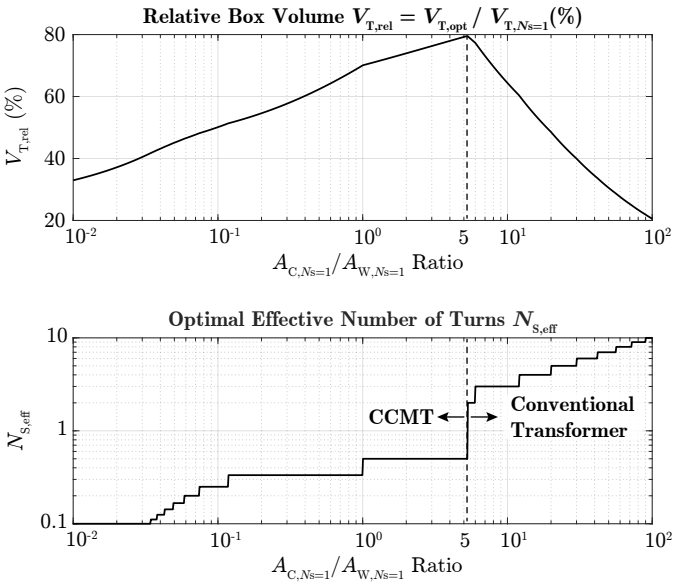


**Fig. 6.** Ratio of the box volume of the smallest transformer $V_{\mathrm{T,opt}}$ to that of a conventional transformer with a single-turn secondary winding $V_{\mathrm{T,Ns=1}}$ for different electrical specifications, along with the corresponding optimal effective number of turns $N_{\mathrm{S,eff}}$ of the secondary winding.

Furthermore, this structure can be expanded as desired by adding additional magnetic return paths in line with winding $S_2$, each with its separate secondary winding. This is exemplified in **Fig. 4c** for three secondary windings, but any number of secondary windings can theoretically be used. However, the first secondary winding $S_1$ is always wound around all windings, which, due to the structure and the special magnetic coupling in the transformer, leads to the complete compensation of the two antiparallel currents on each winding section and, therefore, minimal HF conduction losses.

To roughly estimate for which specifications a CCMT tends to result in more compact designs than a conventional transformer, the approximately expected box volume of the different approaches can be assessed (see **Appendix A**). Subsequently, the best possible transformer volume $V_{\mathrm{T,opt}}$ can be compared with that of a conventional transformer with a single-turn secondary winding ($V_{\mathrm{T,Ns=1}}$) in order to estimate the sensitivity of the transformer volume with regard to the number of effective turns of the secondary winding $N_{\mathrm{S,eff}}$. This is shown in **Fig. 6** for different $A_{\mathrm{C,Ns=1}}$ to $A_{\mathrm{W,Ns=1}}$ ratios, which are given by the specifications of the application according to

$$\frac{A_{\mathrm{C,Ns=1}}}{A_{\mathrm{W,Ns=1}}} = \frac{V_{\mathrm{S}}}{I_{\mathrm{S}}} \cdot \frac{1}{f_{\mathrm{sw}}} \cdot \frac{J_{\mathrm{max}}}{4 \cdot B_{\mathrm{sat}}}. \tag{9}$$

Thus, for area ratios larger than approximately 5, it is more promising to use a conventional transformer, whereas for area ratios smaller than 5, CCMTs seem to be more suitable. The same graph also provides the corresponding optimal $N_{\mathrm{S,eff}}$, where a $N_{\mathrm{S,eff}} = 1/x_{\mathrm{MT}} < 1$ indicates that a CCMT with $x_{\mathrm{MT}}$

**TABLE I**
EXEMPLARY SPECIFICATIONS.

| $V_S$ | $I_S$ | $J_{max}$ | $B_{sat}$ |
|---|---|---|---|
| 10 V | 100 A | 6 A mm$^{-2}$ | 300 mT |

parallel secondary windings should be used.

Considering the exemplary specifications from **Tab. I** and (9), it is possible to directly estimate above which switching frequency $f_{sw,MT}$ it makes sense to consider the use of a CCMT:

$$\frac{V_S}{I_S}\cdot\frac{1}{f_{sw,MT}}\cdot\frac{J_{max}}{4\cdot B_{sat}}=\frac{500000}{f_{sw,MT}}\approx 5\rightarrow f_{sw,MT}=100\,\text{kHz}. \quad (10)$$

Thus, for the given specifications, if switching frequencies above 100 kHz are targeted, a CCMT should be employed, whereas for switching frequencies lower than 100 kHz a conventional transformer might be more promising.
Even though $f_{sw,MT}$ is not a strict boundary due to the simplified calculation of the box volume and may vary in a real application depending on the practical implementation of the CCMT, this value helps to determine what kind of optimal transformer design the specifications will most probably lead to.

Even though it has been shown in this section that CCMTs bring various advantages in low-voltage/high-current applications by expanding the design space for the effective number of secondary side turns $N_{S,eff}$ towards fractional turns, the vast majority of matrix transformers used in today's applications are of the CVMT type. These types of transformers are used for purely practical reasons, as they do not affect the effective voltage transformation ratio (cf. (8)) but lead to significantly more compact and efficient high-current/high-frequency transformer designs compared to conventional transformer structures. This will be explained in more detail in the following based on a simplified transformer design sequence.

## V. OPTIMAL DESIGN OF COMMON-VOLTAGE MATRIX TRANSFORMERS

To design the most compact transformer, it is necessary to minimize both the volume of the core (i.e., the required core cross-sectional area $A_C$) and the volume of the winding (i.e., the required winding window $A_W$). To minimize the core cross-sectional area $A_C$, a secondary-side number of turns $N_S > 1$ could be used, which however is not suitable in high-current/low-voltage applications where there is anyway already a mismatch between the required winding window and core cross-sectional area (cf. **Fig. 3b**). Alternatively, a high switching frequency is often sought, due to the advantageous scaling of the flux linkage $\psi_{pk}$ with the switching frequency (cf. **Fig. 7a**), as one intuitively expects an inversely proportional decrease in the core cross-sectional area $A_C$ with an increase in the switching frequency, according to

$$A_C=\frac{\psi_{pk}}{N_S\cdot B_{max}}=\frac{V_S}{4\cdot f_{sw}\cdot N_S\cdot B_{max}(f_{sw})}. \quad (11)$$

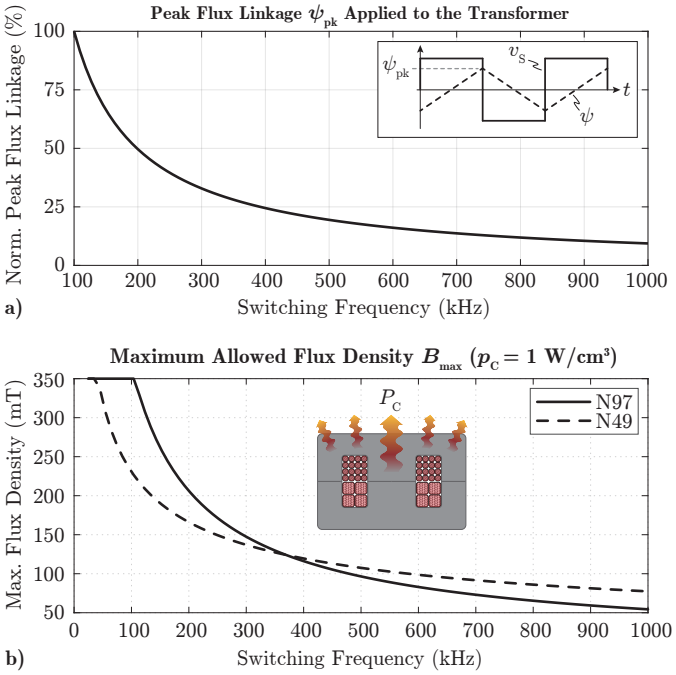


**Fig. 7. (a)** Normalized peak values of the secondary-side flux linkage $\psi_{pk}$ for rectangular voltages $v_S$ and an increasing switching frequency $f_{sw}$, and **(b)** the maximum permissible flux density $B_{max}$ for various ferrite materials considering an exemplary maximum allowed core loss density of 1 W cm$^{-3}$.

However, this holds true only at relatively low frequencies ($< 100$ kHz), since the maximum permissible flux density $B_{max}$ of a core material at high frequencies is no longer determined by saturation but due to the maximum allowable core loss density $p_C$ in the core material (cf. **Fig. 7b**). Even though $p_C$ strongly depends on the core geometry and the transformer's cooling method, a reference value of approximately 1 W cm$^{-3}$ can serve as an initial rough estimate across various core geometries and commercially available core sizes (ELP, pot core, etc.). If the thermal limitation is considered instead of the saturation flux density of a core material at high frequencies, one still observes an

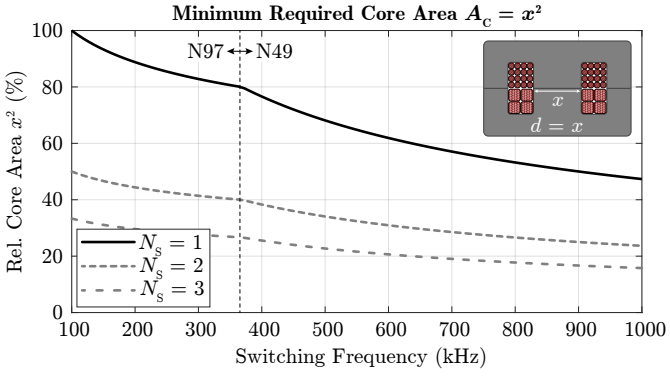


**Fig. 8.** Scaling of the required core cross-sectional area $A_C$ (square cross-section with width $x$) for different secondary-side numbers of turns $N_S$ and different switching frequencies $f_{sw}$, where the most suitable core material is used for each case.

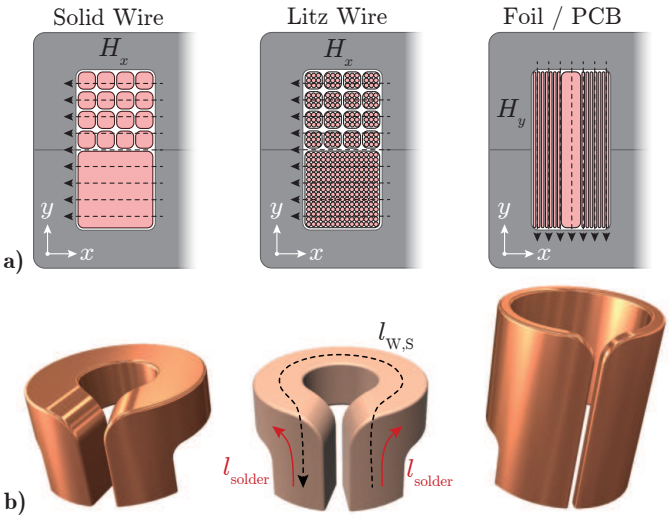


**Fig. 9. (a)** Cross-sectional view of the winding window of a transformer with two windings made of solid wire, litz wire, or copper foils, with the simplified path of the main magnetic field illustrated by dashed arrows. **(b)** Termination of the secondary-side single-turn windings for the three winding technologies, with none of them considered a practical solution for real applications.

advantageous scaling of $A_{\mathrm{C}}$ for higher frequencies, but the required cross-sectional area decreases significantly more slowly (cf. **Fig. 8**). If the switching frequency is e.g. doubled from 100 kHz to 200 kHz, according to **Fig. 7a**, a reduction of $A_{\mathrm{C}}$ by 50 % would be expected. However, the thermal limitation of $B_{\mathrm{sat}}$ results in a decrease of $A_{\mathrm{C}}$ by only about 10 % (cf. **Fig. 8**). Nevertheless, it generally holds true that an increase in the switching frequency has a positive impact on the core volume. However, this does not apply to the winding volume, as will be explained in the following.

An increase in the switching frequency has a dual impact on the winding volume or the efficiency of the copper windings. On the one hand, the required core cross-sectional area is reduced, leading to shorter average winding lengths, which positively affects the DC resistance of the windings. On the other hand, adverse high-frequency effects (skin and proximity effects) are also intensified [7]. This results in the available winding window $A_{\mathrm{W}}$ being less effectively utilized, tending to increase in size. This becomes particularly evident in high-current applications, where very large copper cross-sections of the turns are needed for efficient transformer operation. However, in the case of conventional solid-wire windings, large copper surfaces are automatically exposed to the leakage field within the winding window, leading to significant HF conduction losses due to the induced eddy currents. This is simplistically shown in **Fig. 9a**, taking into account that in a transformer, the stray field dominates in one dimension (in this case, in the $x$-direction), and the fields in the other dimensions can largely be neglected.
There are different approaches that usually aim to minimize the HF effects as much as possible, which can only be achieved by minimizing the electrically connected copper surfaces exposed to the leakage fields. One approach involves the use of litz wire windings, where multiple parallel-connected and specially twisted individual conductors (strands) in a winding result in minimal electrically connected copper areas exposed to the leakage fields (cf. **Fig. 9a**). However, this approach is often not effective for single-turn windings with large required copper cross-sections for two reasons. On the one hand, a litz wire with a certain outer diameter $d_{\mathrm{litz}}$ requires a minimum length $l_{\mathrm{pitch}}$, known as the length of lay, to function effectively and reduce the HF conduction losses as desired. This minimum length can be estimated as $l_{\mathrm{pitch}} = 25 \cdot d_{\mathrm{litz}}$ [8], and is often not achieved in high-current applications (large $d_{\mathrm{litz}}$) with a single-turn winding (cf. $l_{\mathrm{W,S}}$ in **Fig. 9b**). On the other hand, terminating a litz wire winding with large $d_{\mathrm{litz}}$ is mechanically extremely challenging, not least because the heat from soldering the litz wire to the PCB destroys the insulation between the individual strands over a certain length $l_{\mathrm{solder}}$, further reducing the effective length of the litz wire where it reduces the HF conduction losses (cf. **Fig. 9b**).
Alternatively, for high-current applications, foil windings are often used. While they theoretically belong to solid-wire windings, their altered form factor, specifically the elongation of the copper cross-section into a thin rectangle, minimizes the copper surface exposed to the leakage fields (cf. **Fig. 9a**). The foil is stretched to the extent that its thickness $h_{\mathrm{foil}}$ allows for neither significant skin-effect losses ($F_{\mathrm{F}}$) nor significant proximity-effect losses ($G_{\mathrm{F}}$), thereby only minimally increasing the resistance of the winding for higher switching frequencies, according to

$$R_{\mathrm{HF}} = R_{\mathrm{DC}} \cdot \left( 2F_{\mathrm{F}} + 2G_{\mathrm{F}} \left( \frac{H_{\mathrm{prox,rms}}}{I_{\mathrm{rms}}} \right)^2 \right), \qquad (12)$$

where $R_{\mathrm{DC}}$, $F_{\mathrm{F}}$, $G_{\mathrm{F}}$, $H_{\mathrm{prox,rms}}$ and $I_{\mathrm{rms}}$ denote the DC resistance of a winding, the skin effect loss factor, the proximity effect loss factor, the rms value of the external leakage field though a winding and the rms value of the current in a winding, respectively [9] (cf. **Fig. 10**). Thus, the relative foil thickness $\nu = h_{\mathrm{foil}}/\delta$, where $\delta$ denotes the frequency dependent skin depth, should not exceed a value of approximately 1 to 1.5, such that the HF conduction losses can be kept low. Consequently, the permissible foil thickness $h_{\mathrm{foil}}$ becomes thinner with increasing frequency $f_{\mathrm{sw}}$ (cf. **Fig. 10**). However, this automatically leads to the necessity of using a wider foil ($b_{\mathrm{W}}$) since the required copper cross-sectional area does not change with the frequency. This is illustrated in **Fig. 10** for an exemplary secondary current of $I_{\mathrm{S}} = 100\,\mathrm{A}$ and a maximum current density of $50\,\mathrm{A\,mm^{-2}}$. Since terminating a wide foil is both mechanically challenging and comparably lossy (cf. **Fig. 9b**), instead of the vertical foil winding in **Fig. 9a**, a horizontal PCB winding in combination with, e.g., a pot core, is often preferred (cf. **Fig. 11**). This arrangement simplifies the termination of the windings and also reduces the resulting manufacturing costs.

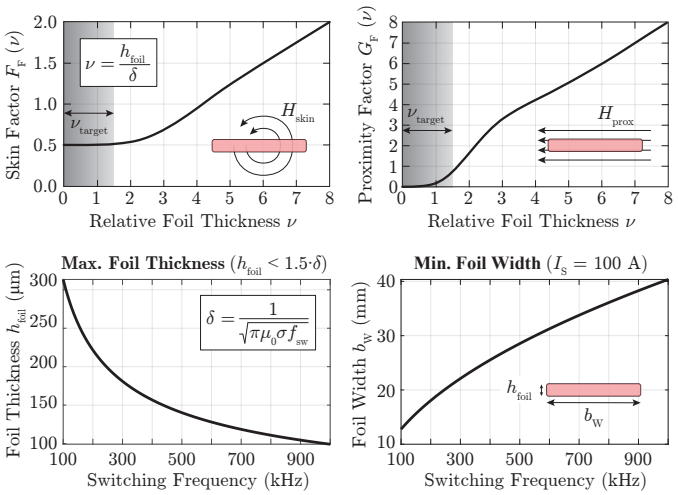


**Fig. 10.** Skin effect loss factor $F_F$ as well as proximity effect loss factor $G_F$ for different normalized foil thicknesses $\nu$. Furthermore, the maximum permissible foil thickness $h_{foil}$ is shown for different switching frequencies, which largely prevents considerable high-frequency conduction losses in the Windings. Additionally, the minimum foil width $b_W$ is indicated for an exemplary secondary winding current $I_S$ of 100 A and a maximum current density of 50 A mm$^{-2}$.

Due to the increasingly wider foil required at higher switching frequencies and the almost negligible reduction in the core cross-sectional area in comparison, the overall diameter $d_T$ of the transformer, as well as its volume $V_T$, increases for higher frequencies.

To counteract this disadvantageous scaling with increasing frequency, it would be necessary to reduce the required foil width $b_W$, allowing for a reduction in the overall diameter $d_T$ and, consequently, the volume. However, this can only be achieved by dividing the secondary single-turn winding into multiple single-turn sub-windings, arranged above or next to each other, and then connecting them in parallel. In other words, considering the use of a common-voltage matrix transformer (CVMT). This is illustrated in **Fig. 12** for $M = 2$ and $M = 4$ secondary-side sub-windings arranged side-by-side, where it can be observed that while the total core cross-sectional area $A_{C,tot}$ in the PCB plane increases ($A_{C,tot}(M) = M \cdot A_{C,tot}(1)$)), the total copper area is significantly reduced. Overall, the box volume of the entire transformer usually decreases with the number of parallel-connected sub-windings $M$, especially at high frequencies (cf. **Fig. 13**). Of course, one could also arrange the secondary sub-windings on top of each other to minimize the overall footprint of the transformer. However, this arrangement would require an expensive PCB with many layers and prevent the rectifier components from being directly integrated into the sub-windings, as proposed in [10], leading to a significantly lossier termination of the windings. For this reason, the side-by-side arrangement is usually preferred, despite the larger footprint.

Even though the use of a large number of sub-windings $M$ can mitigate the disadvantageous scaling of the transformer box volume with the switching frequency, it is still evident that in high-current/low-voltage applications, increasing the switching frequency for reducing the volume of a PCB-winding transformer may not necessarily be worthwhile, especially when the effective number of turns of the secondary winding $N_{S,eff}$ is not optimally chosen (e.g., when $N_{S,eff} = 1$ is used, even though an $N_{S,eff} < 1$ would lead to more efficient and compact solutions). Therefore, it might be necessary to use a combination of CCMT and CVMT structures if high switching frequencies are to be used, where the CCMT approach is employed to achieve the $N_{S,eff}$ that is optimal

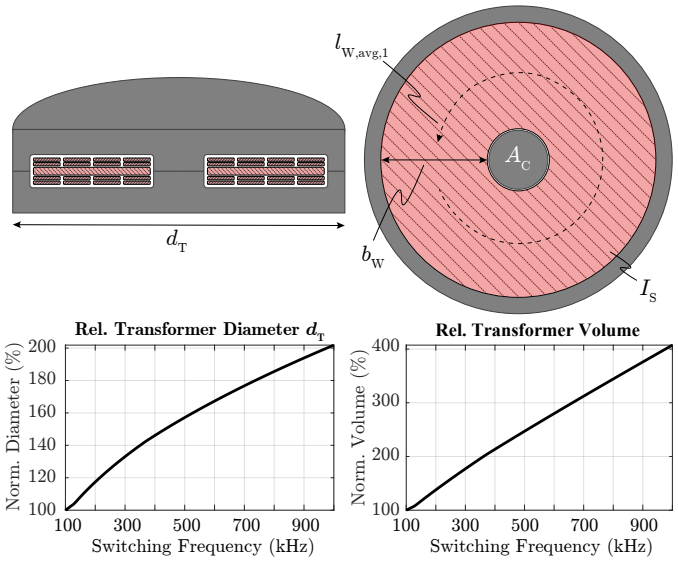


**Fig. 11.** Cross-section and top view of a pot-core PCB-winding transformer with a single secondary winding, as well as the scaling laws of the normalized transformer diameter $d_T$ and the normalized transformer volume $V_T$ for the exemplary specifications of **Tab. I** but with a maximum current density of 50 A mm$^{-2}$.

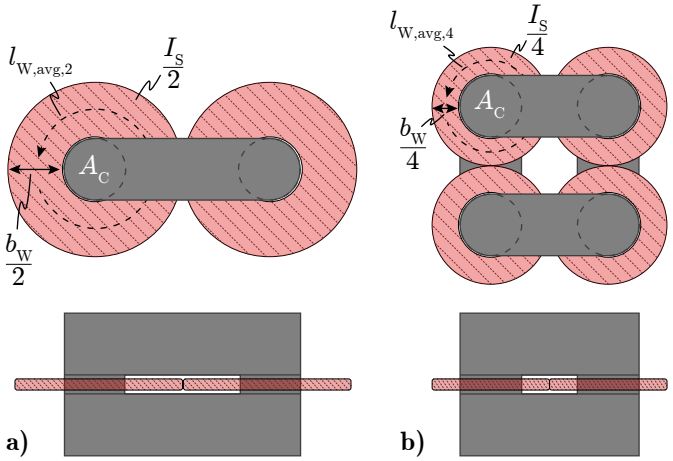


**Fig. 12.** **(a)** Top view and cross-section of a PCB-winding matrix transformer with two ($M = 2$) parallel-connected single-turn secondary windings, and **(b)** the same, but for four ($M = 4$) parallel-connected secondary single-turn windings, both for the exemplary specifications of **Tab. I** but with a maximum current density of 50 A mm$^{-2}$.

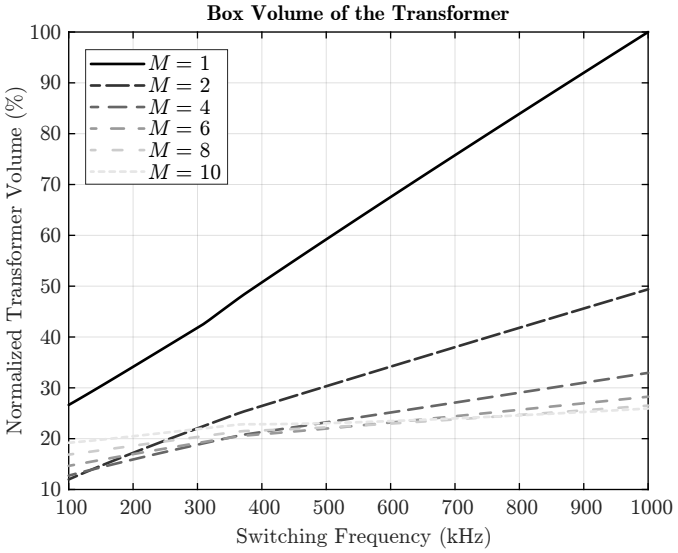


**Fig. 13.** Scaling of the normalized box volume of the PCB-winding CVMT for different switching frequencies $f_{\mathrm{sw}}$, different numbers of secondary single-turn windings $M$ and the exemplary specifications of **Tab. I**.

from a power density perspective, while the CVMT approach is used to implement the secondary turns of the CCMT as efficiently and compactly as possible.

However, in addition to reducing the box volume of the transformer when a CVMT with $M > 1$ is used, there is another significant advantage of employing a CVMT: the DC resistance of the windings is significantly reduced. This is because the total copper cross-section of the secondary winding remains constant regardless of $M$, while the average length $l_{\mathrm{W,avg,M}}$ of the windings is considerably shortened (cf. **Fig. 11** and **Fig. 12**). Consequently, the conduction losses in the transformer can be reduced, leading to a significant increase in its efficiency (cf. **Fig. 14**). This is the main reason why CVMTs with a high number of $M$ are often found in contemporary high-current applications, where cost-effective PCB-winding transformers are employed.

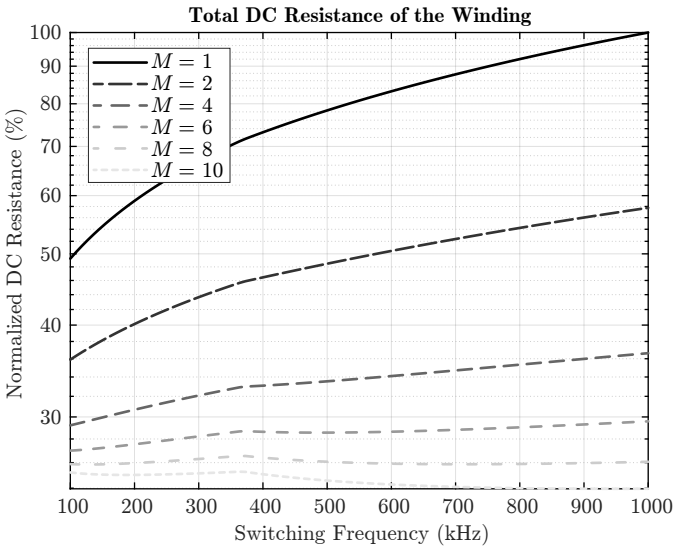


**Fig. 14.** Scaling of the normalized DC resistance of the PCB-winding CVMT for different switching frequencies $f_{\mathrm{sw}}$, different numbers of secondary single-turn windings $M$ and the exemplary specifications of **Tab. I**.

## VI. Conclusion

In conclusion, this paper presented an overview of two distinct types of matrix transformers (common-voltage and common-current matrix transformers, i.e., CVMTs and CCMTs) and conducted a comprehensive analysis of their influence on the electromagnetic behavior of a transformer structure in comparison to conventional transformer arrangements. Additionally, it has been shown how, through simple specification-based assessments, one can easily determine the suitability of employing a CCMT to address potential disparities between the necessary copper area and core cross-sectional area of a conventional transformer, commonly found in converter systems for data centers or electric vehicles, which transfer energy from a high-voltage supply (400 V to 800 V) to low-voltage (12 V to 24 V) loads. Finally, a thorough investigation of the practical advantages associated with CVMTs has been presented, emphasizing their positive impact on the overall efficiency and power density of the magnetic component in the aforementioned applications.

## References


[1] R. W. Erickson and D. Maksimovic, *Fundamentals of Power Electronics*. Springer Cham, 2020. [Online]. Available: https://doi.org/10.1007/978-3-030-43881-4

[2] J. G. Kassakian, D. J. Perreault, G. C. Verghese, and M. F. Schlecht, *Principles of Power Electronics*, 2nd ed. Cambridge University Press, 2023.

[3] M. Mogorovic and D. Dujic, "100 kw, 10 khz medium-frequency transformer design optimization and experimental verification," *IEEE Transactions on Power Electronics*, vol. 34, no. 2, pp. 1696–1708, 2019.

[4] E. Herbert, *Design and application of matrix transformers and symmetrical converters*. FMTT, Incorporated, 1990.

[5] C. Fei, F. C. Lee, and Q. Li, "High-efficiency high-power-density llc converter with an integrated planar matrix transformer for high-output current applications," *IEEE Transactions on Industrial Electronics*, vol. 64, no. 11, pp. 9072–9082, Nov 2017.

[6] M. J. Kasper, L. Peluso, G. Deboy, G. Knabben, T. Guillod, and J. W. Kolar, "Ultra-high power density server supplies employing gan power semiconductors and pcb-integrated magnetics," in *CIPS 2020; 11th International Conference on Integrated Power Electronics Systems*, 2020, pp. 1–8.

[7] Z. Ouyang and M. A. E. Andersen, "Overview of planar magnetic technology—fundamental properties," *IEEE Transactions on Power Electronics*, vol. 29, no. 9, pp. 4888–4900, 2014.

[8] H. L. Wire, "Litz wire calculation and design," 2024, accessed: 2024-06-13. [Online]. Available: https://www.hflitzwire.com/litz-wire-calculation-and-design/

[9] J. A. Ferreira, *Eddy Currents in Conductors*. Boston, MA: Springer US, 1989, pp. 49–65. [Online]. Available: https://doi.org/10.1007/978-1-4757-2014-3˙4

[10] D. Huang, S. Ji, and F. C. Lee, "Llc resonant converter with matrix transformer," *IEEE Transactions on Power Electronics*, vol. 29, no. 8, pp. 4339–4347, 2014.

## APPENDIX

### A. Box Volume Calculations

In order to estimate the scaling of the size of a transformer, it makes sense to calculate the respective box volume $V_\mathrm{T}$, where it is assumed that both, the core cross-sectional area as well as the winding windows are squares with $x_\mathrm{C}$ and $x_\mathrm{W}$ representing their respective side lengths.
For conventional transformer configurations (single primary and secondary winding), the required winding window $A_\mathrm{W}$ and core cross-sectional area $A_\mathrm{C}$ can be calculated according to

$$A_\mathrm{W} = \frac{2 \cdot N_\mathrm{S} \cdot I_\mathrm{S}}{J_\mathrm{max}} \quad \text{and} \quad A_\mathrm{C} = \frac{V_\mathrm{S}}{2 \cdot f_\mathrm{sw} \cdot N_\mathrm{S} \cdot B_\mathrm{max}}, \tag{13}$$

respectively. Thus, the respective side lengths $x_\mathrm{C}$ and $x_\mathrm{W}$ are given as

$$x_\mathrm{W} = \sqrt{A_\mathrm{W}} \quad \text{and} \quad x_\mathrm{C} = \sqrt{A_\mathrm{C}}. \tag{14}$$

The box volume $V_\mathrm{T}$ can then be calculated according to

$$V_\mathrm{T} = 2 \cdot (x_\mathrm{C} + x_\mathrm{W}) \cdot (x_\mathrm{C} + 2x_\mathrm{W}) \cdot (2x_\mathrm{C} + x_\mathrm{W}), \tag{15}$$

as illustrated in **Fig. 15**.

In a CCMT, the core cross-sectional area per secondary sub-winding can be calculated as

$$A_\mathrm{C} = \frac{V_\mathrm{S}}{2 \cdot f_\mathrm{sw} \cdot B_\mathrm{max}}, \tag{16}$$

which is why the side lengths of one core leg $x_\mathrm{C}$ is given as

$$x_\mathrm{C} = \sqrt{A_\mathrm{C}}. \tag{17}$$

The required area of one winding window depends on the number of secondary sub-windings $x_\mathrm{MT}$ and can be calculated according to

$$A_\mathrm{W} = \frac{2 \cdot I_\mathrm{S}}{J_\mathrm{max} \cdot x_\mathrm{MT}}. \tag{18}$$

In order to calculate the box volume of the CCMT, it is necessary to calculate the missing dimensions $\alpha$, $\beta$ and $\gamma$ which are depicted in **Fig. 16**. These dimensions can be calculated according to

$$\alpha = (x_\mathrm{MT} - 1) \cdot x_\mathrm{C} + (x_\mathrm{MT} - 2) \cdot x_\mathrm{W}, \tag{19}$$

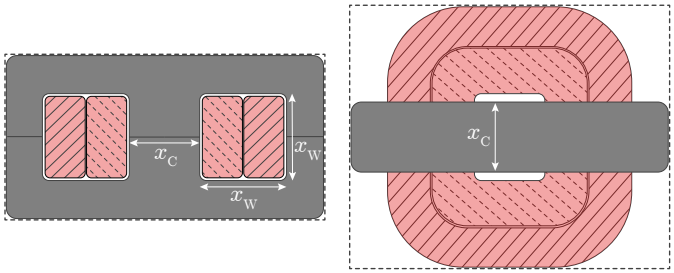


**Fig. 15.** Dimensions of a conventional transformer with square core cross-sectional areas and winding windows, which are needed for calculating the box volume of the transformer, where the dashed rectangles represent the outer dimensions of the box.

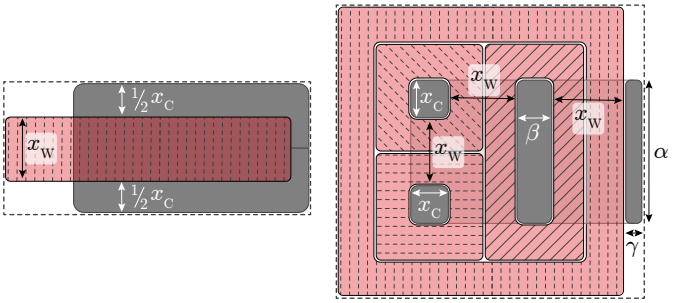


**Fig. 16.** Dimensions of a common-current matrix transformer (CCMT) with square core cross-sectional areas of the return paths and square winding windows, which are needed for calculating the box volume of the transformer. The dashed rectangles represent the outer dimensions of the box.

$$\beta = \frac{x_\mathrm{MT} \cdot A_\mathrm{C}}{\alpha}, \tag{20}$$

and

$$\gamma = \frac{A_\mathrm{C}}{\alpha}. \tag{21}$$

Finally, the box volume of the CCMT is given as

$$V_\mathrm{T} = (x_\mathrm{C} + x_\mathrm{W}) \cdot \tag{22}$$
$$(x_\mathrm{MT} \cdot x_\mathrm{W} + (x_\mathrm{MT} - 1) \cdot x_\mathrm{C}) \cdot \tag{23}$$
$$(3 \cdot x_\mathrm{W} + x_\mathrm{C} + \beta + \gamma). \tag{24}$$